International Journal of Engineering and Advanced Technology (IJEAT)
ISSN: 2249-8958 (Online), Volume-9 Issue-1, October, 2019

Modified Variable Step Size Affine Algorithm for Grid Integrated PV System

Byomakesh Dash, Satish Choudhury, Renu Sharma

***Abstract:** This paper proposes a Modified Variable Step Size Affine (MVSA) algorithm for a single stage grid integrated photovoltaic (GIPV) system. Integration of photovoltaic (PV) system to utility grid encounters many control issues like nonlinearities, disturbances and unbalanced loading. The proposed algorithm not only improves the overall performance of the system despite all the adverse conditions but also improves the power quality as per IEEE-519 standard. The proposed algorithm is developed to eliminate harmonics caused by nonlinear loads, to transfer active power from PV source to load as well as to grid under unity power factor condition, to maintain constant voltage profile at the point of common coupling and to provide a controlled reference signal to the hysteresis controller so as to produce suitable gate pulse to voltage source converter (VSC). In this paper, a PI control is used to maintain dc link voltage and P&O method is used to extract optimum power from PV source irrespective of all disturbances in the utility grid. The system under consideration is modelled and simulated using MATLAB/Simulink software. Comparing the performances of the said variable step size control algorithm with that of fixed step size algorithm like Fixed Step Size Affine (FSA) Projection Algorithm and Least Mean Fourth (LMF), it is observed that the mean square error in MVSA is less as compared to FSA and LMF.*

***Keywords:** Fixed Step Size Affine (FSA) Projection algorithm, Modified Variable Step Size affine (MVSA) algorithm, Photovoltaic (PV), Perturb& Observe (P&O), Total Harmonics Distortion (THD)*

I. INTRODUCTION

The major challenges in 21st century is global warming, changing climate caused by greenhouse effect and effective use of natural resources which are in declining state. This forces the world community to think for some alternative form of clean energy for the future generation. The best way to achieve this is to adopt solar energy as the alternative to the conventional energy which is clean, secure and abundantly available. Again the cost of photovoltaic module has reduced by 60% from 2011-2013 and will further reduce by 40% by 2020[1].This reduced cost and environment friendly nature of photo voltaic system has attracted many researchers to work in the direction of integrating photovoltaic sources to utility grid, which leads to new and innovative integrating process. Power electronics conversion plays a vital role for integrating photovoltaic sources to utility grid and to improve its efficiency. It adopts the system continuously and draw maximum power from photovoltaic sources irrespective of weather and load conditions. Normally this task is performed by MPPT techniques, and there is substantial literature on MPPT techniques in [2]-[9]. The literature reveals broad work has been done to model sun powered photovoltaic systems [2] and to extract maximum power from it such as perturb and observe (P&O) [3], INC [4], variable step size incremental resistance [5], artificial bee colony algorithm [6] and many more intelligent control techniques such as reinforcement learning (RL), fuzzy logic, neural network and genetic algorithm [7]-[9]. Integration of photovoltaic systems to utility grid can be realized in two stages of power conversion. First one is dc/dc converter with MPPT control and second one is dc/ac inverter. Literature reveals that single stage power conversion is more efficient as compared to two stage conversion [10].The factors to be considered while integrating solar photovoltaic systems to grid are degraded power quality, performance and stability under load unbalancing, harmonics and reliability .Hence the power electronics converter require a robust control logic that work satisfactorily under various issues mentioned above and disturbances at the load as well as grid end. Signal processing based many adaptive algorithms have been cited in the literature, such as recursive least square [11], DFT, droop control [12], LMF [13], Least mean square (LMS) [14], DNLMS, modified VSS-LMS, variable leaky LMS [15], along with the conventional techniques such as SRF, ILST [16], IRPT, enhanced phase locked loop etc. Main objective of these algorithms are to reject the harmonics accurately and to get desired response in adverse conditions. An affine projection algorithm [17] is proposed in the literature that is based on affine subspace projections. As step size parameters govern the convergence rate and stability of classical affine projection algorithm (APA), numerous variable step size affine projection algorithms were developed and proposed in the literature [18]-[21]. Main feature of these algorithms are fast convergence rate, low steady state mean square error and low computational complexity. In this paper, a modified variable step size affine (MVSA) is proposed in grid synchronization process to estimate the active and reactive current components of three phase nonlinear loads. These active components are

Revised Manuscript Received on October 30, 2019.
* Correspondence Author
Byomakesh Dash*, EE, Siksha 'O' Anusandhan (Deemed to be University) , Bhubaneswar, India. Email: byomakesh19@gmail.com
Satish Choudhury, EE, Siksha 'O' Anusandhan (Deemed to be University), Bhubaneswar, India.
Renu Sharma, EE, Siksha 'O' Anusandhan (Deemed to be University), Bhubaneswar, India.

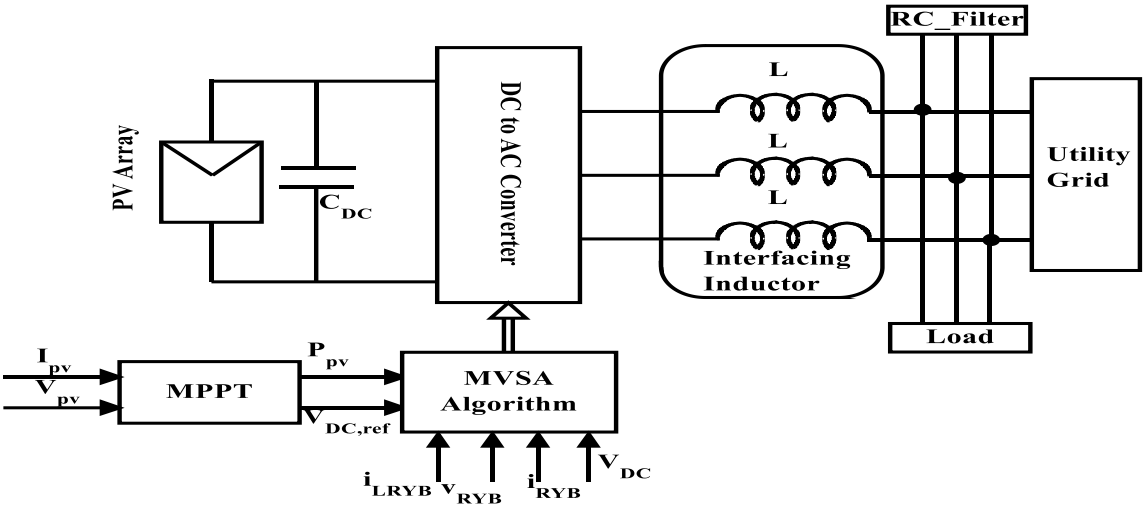

Fig. 1 Proposed system topology

used to generate reference grid currents. In the proposed algorithm, a step size scalar is applied to update the step size, so as to improve its behaviour under steady as well as dynamic conditions. The grid integrated photovoltaic system with the proposed algorithm is designed, modelled and simulated under nonlinear loads in unity power factor (UPF) mode under various dynamic conditions in MATLAB/SIMULINK environment and is compared with the conventional fixed step methods to evaluate its effectiveness.

This paper contributes in modification of control algorithm for generating reference grid current to maintain the performance parameters at its set value. This work basically modify the Affine algorithm by using an exponential step size scalar function along with a variable step size. The modified step size helps to reduce mean square error and oscillation in steady state and transient state under nonlinear loading condition. The step size scalar improves the convergence rate of MVSA based algorithm as compared to FSA and LMF algorithm.

The rest of the paper is organised as follows: Section II describes the modelling and design of photovoltaic system. Section III describes the control algorithm. Section IV describes the result analysis using MATLAB/SIMULINK. Section V conclude this paper.

II. MODELLING AND DESIGN OF GRID INTEGRATED PV SYSTEM

The configuration of the grid connected PV system is shown in Fig.1. It comprises of a PV array, DC link capacitor (CDC), Interfacing Voltage source converter (VSC), R-C ripple filter, interfacing inductors (L), and nonlinear load. Interfacing inductor compensates the harmonics present in the grid current, whereas R-C ripple filter mitigates the switching ripple at the point of inter section. Power flow from source to grid as well as to load is governed by thee single stage PV topology. The nonlinear load is modelled by an uncontrolled diode bridge rectifier with an R-L load. Maximum power from the PV source is extracted using P&O method.

A. Modelling of Solar Photovoltaic Array and determination of System Parameters.

Villava et al. [2] describe in detail the modelling of PV array composed of several basic modules connected in series and parallel. A PV module consists of number of cells in it. A number of PV modules connected in series and parallel to form a PV array.

The PV system designed here is of 50 kW connected to a 415 V, 50 Hz, three phase system. The number of series and parallel connected PV modules required to meet the design criterion are calculated as follows:

$$N_s = \frac{V_{DC}}{V_{mp}} = \frac{700}{26.3} = 26.7 \cong 27 \quad (1)$$

$$N_p = \frac{P_{\max}}{V_{DC} I_{mp}} = \frac{50000}{700 \times 7.61} = 9.386 \cong 10 \quad (2)$$

The value of DC bus voltage is calculated as

$$V_{DC} = \frac{2V_{Lm}}{\sqrt{3}k} = \frac{2\sqrt{2} \times 415}{\sqrt{3} \times 1} = 677.69 \quad (3)$$

where V_{Lm} is the peak line voltage of the grid and k is the modulation index. The value of DC bus voltage is taken as 700 volt.

The value of interfacing inductance is calculated as [22]

$$L = \sqrt{3}\frac{mV_{DC}}{12h_0 f_{SW} \Delta I} = \frac{\sqrt{3} \times 1 \times 700}{12 \times 1.2 \times 10000 \times 0.03 \times 71.43} = 3.9mH \cong 4mH \quad (4)$$

Where h_0 is the overloading factor, f_{SW} is the switching frequency, and ΔI is the percent (3%) of ripple current.

The voltage source converter DC link capacitance is computed as

$$C_{DC} = \frac{P_{DC}}{2V_{DC}\omega V_{DCrip}} = \frac{50000}{2\times 700\times 314\times 0.02\times 700}$$

$$= 8124.3\mu F \quad (5)$$

Where V_{DCrip} is percentage of ripple voltage and ω is the angular frequency. The ripple filter is designed with capacitance $C_{rf} = 10\mu F$ and resistance $R_f = 5\Omega$ respectively [22].

III. CONTROL ALGORITHM

Integration of a PV system to utility grid can be realized in two stages. First one is MPPT algorithm, which helps to track maximum power from photovoltaic sources and gives reference voltage so as to maintain the dc bus voltage at its desired value. The second one is the control algorithm for VSC which one is responsible for generating gate pulses for the controlled solid-state switches of VSC

The reference voltage thus produced in stage one is compared with the actual voltage obtained across the dc link capacitor and the error is fed to PI controller to produce the dc power loss component. The peak voltage is determined from in phase and quadrature component of the unit templates. Then the active and reactive weight components are estimated using MVSA algorithm as shown in fig.2 using the dc and ac loss components followed by the calculation of resultant weight. The resultant weight thus calculated is then utilized to produce harmonic free reference grid currents and subsequently they produce suitable pulse signal for VSC. These estimated weights are used to control the current flowing in the system so as to maintain the power flow from source end to utility grid and load. Further the proposed algorithm is well capable to, minimize the effect of harmonics in the load current, noise, load unbalancing and transfer power under unity power factor condition.

A. Estimation of Unit Templates and Amplitudes of Terminal Voltage.

Phase voltages (v_R, v_Y, v_B) can be computed from line voltages (v_{RY}, v_{YB}) as per the following equations [23]

$$v_R = \frac{2}{3}v_{RY} + \frac{1}{3}v_{YB}$$

$$v_Y = \frac{-1}{3}v_{RY} + \frac{1}{3}v_{YB} \quad (6)$$

$$v_B = \frac{-1}{3}v_{RY} - \frac{1}{3}v_{YB}$$

Peak value of terminal voltage can be computed as follows

$$V_p = \frac{2}{3}\sqrt{\sum_{x=R,Y,B} v_x^2} \quad (7)$$

The in-phase and quadrature unit templates are calculated as [24]

$$u_{ax} = \frac{v_x}{V_p} \quad (8)$$

where x represents R, Y and B phases and u_{ax} is in-phase active unit template of respective phases.

$$u_{bR} = \frac{1}{\sqrt{3}}\left(-u_{aY} + u_{aB}\right),$$

$$u_{bY} = \frac{1}{2\sqrt{3}}\left(3u_{aR} + u_{aY} - u_{aB}\right) \quad (9)$$

$$u_{bB} = \frac{1}{2\sqrt{3}}\left(-3u_{aR} + u_{aY} - u_{aB}\right)$$

where u_{bR}, u_{bY}, u_{bB} represents quadrature unit template.

B. Estimation of AC and DC Loss Component

The difference between reference voltage provided by MPPT control (V_{DCref}) and voltage across dc link capacitor (V_{DC}) is the dc voltage error and is computed as follows

$$V_{DE}(m) = V_{DCref}(m) - V_{DC}(m) \quad (10)$$

The dc loss component is computed as

$$\delta_{ca}(m) = k_p\left(1 + \frac{k_i}{k_p}\frac{1}{s}\right)V_{DE}(m) \quad (11)$$

where k_p and k_i are proportional and integral gain. Fig.3 shows the block diagram of DC voltage controller. Where gain of the foreword path $G(s)$ and feedback path gain $H(s)$ are represented as

$$G(s) = \frac{sk_p + k_i}{s^2 C_{DC}}, \; H(s) = \frac{\omega_c}{s + \omega_c} \quad (12)$$

Where ω_c is the cut off frequency (10Hz) of the low pass filter in the feedback path.

The ac voltage error is calculated by subtracting peak value of terminal voltage (V_p) from its reference value V_{pref}.

$$V_{pe}(m) = V_{pref}(m) - V_p(m) \quad (13)$$

The ac loss component is computed as

$$\delta_{cb}(m) = k_p\left(1 + \frac{k_i}{k_p}\frac{1}{s}\right)V_{pe}(m) \quad (14)$$

To show the effect of PV system, $\delta_{pv}(m)$ is added to the system and is computed as

$$\delta_{pv}(m) = \frac{2P_{pv}(m)}{3V_p} \quad (15)$$

where P_{pv} is the output power of PV system.

C. Estimation of Active and Reactive Component of Load Current

The respective weight components are updated as follows [17]

$$\delta_{ax}(m+1) = \delta_{ax}(m) + \mu_x'(m)\hat{u}_{ax}\left(\hat{u}_{ax}^T\hat{u}_{ax}\right)^{-1}\hat{e}_{ax}(m) \quad (16)$$

where $\mu_x'(m) = s_x(m)\mu_x(m)$ (17)

Here x represents R, Y and B phases respectively, $\mu_x(m)$ is the variable step size parameter, $s_x(m)$ is the

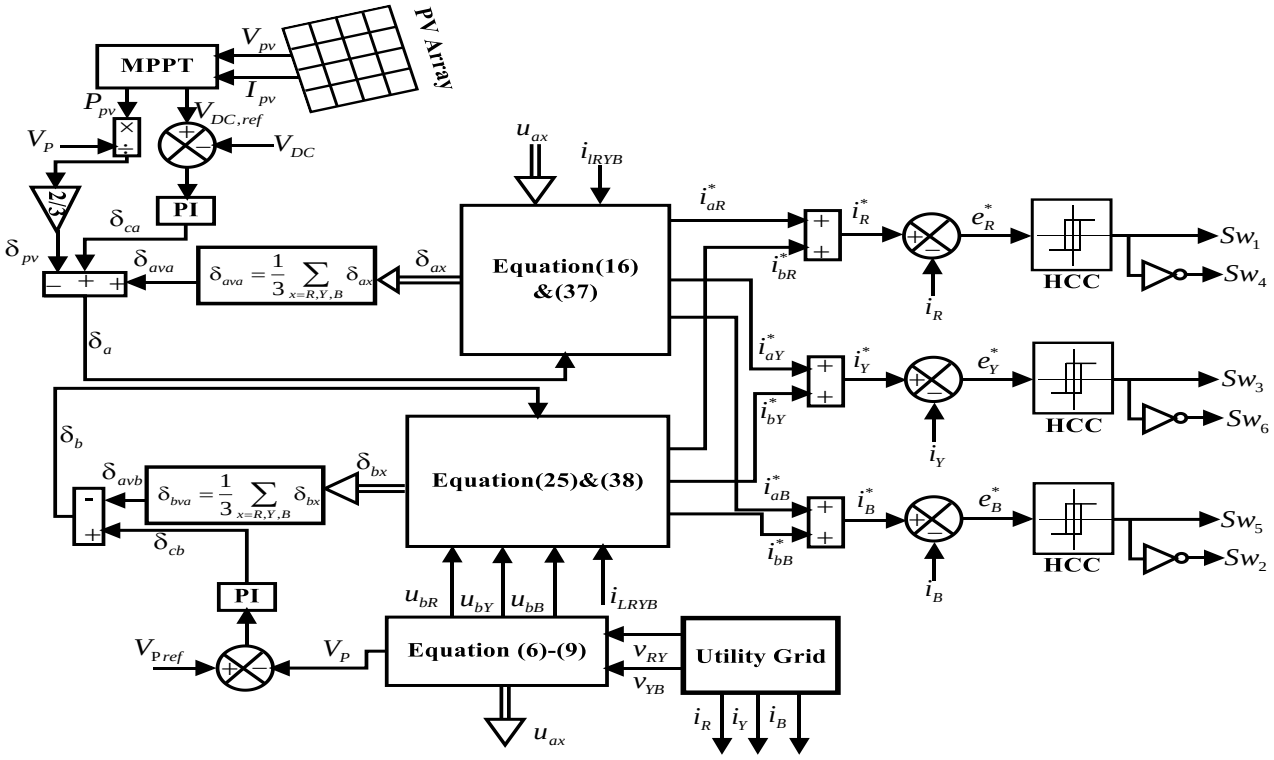

Fig. 2 MVSA algorithm control structure

variable step size scalar and $\hat{e}_{ax}(m)$ is the estimated error. The variable step size parameter $\mu_x(m)$ can be chosen appropriately to get desired result and is represented as: [25]

$$\mu_x(m+1)=\lambda\mu_x(m)+\tau\left\|\hat{p}_x(m)\right\|^2\hat{e}_{ax}^{\,2}(m)$$

(18)

$$\hat{p}_x(m)=\sigma\, p_x(m-1)+(1-\sigma)\hat{u}_{ax}(m)\hat{e}_{ax}(m)$$

(19)

Where, $0<\lambda<1$, $\tau>0$ are tuning parameters and $0<\sigma<1$ is a smoothing factor.

Step size scalar $s_x(m)$ accomplish the role of scaling the step size $\mu_x(m)$ so that the system will function properly due to any disturbance and noise and is represented as

$$s_x(m)=\frac{1}{1+\beta C_x(m)} \qquad (20)$$

Where $\beta>0$.

$$C_x(m)=\hat{e}_{ax}^{\,T}(m)\left(\hat{u}_{ax}^{\,T}\hat{u}_{ax}\right)^{-1}\hat{e}_{ax}(m)$$

(21)

The estimated error is calculated as

$$\hat{e}_{ax}(m)=\hat{i}_{Lx}(m)-\hat{u}_{ax}(m)\delta_{ax}(m)$$

(22)

$$\hat{i}_{Lx}(m)=i_{Lx}(m)-\alpha i_{Lx}(m-1)$$

(23)

$$\hat{u}_{ax}(m)=u_{ax}(m)-\alpha u_{ax}(m-1)$$

(24)

where x represents phases R, Y and B respectively, $i_{Lx}(m)$ is the load current of phases x and $u_{ax}(m)$ is the in phase unit template of respective phases.

Similarly the estimated reactive weight of phases R, Y and B are updated as

$$\delta_{bx}(m+1)=\delta_{bx}(m)+\mu_x'(m)\hat{u}_{bx}\left(\hat{u}_{bx}^{\,T}\hat{u}_{bx}\right)^{-1}\hat{e}_{bx}(m) \qquad (25)$$

Here x represents phases R, Y and B respectively.

$$\mu_x(m+1)=\lambda\mu_x(m)+\tau\left\|\hat{p}_x(m)\right\|^2\hat{e}_{bx}^{\,2}(m)$$

(26)

$$\hat{p}_x(m)=\sigma\,\hat{p}_x(m-1)+(1-\sigma)\hat{u}_{bx}(m)\hat{e}_{bx}(m)$$

(27)

$$s_x(m)=\frac{1}{1+\beta C_x(m)}$$

(28)

$$C_x(m)=\hat{e}_{bx}^{\,T}(m)\left(\hat{u}_{bx}^{\,T}\hat{u}_{bx}\right)^{-1}\hat{e}_{bx}(m) \qquad (29)$$

Retrieval Number: A1881109119/2019©BEIESP
DOI: 10.35940/ijeat.A1881.109119
Journal Website: www.ijeat.org

Published By:
Blue Eyes Intelligence Engineering
& Sciences Publication

$$\hat{e}_{bx}(m) = \hat{i}_{Lx}(m) - \hat{u}_{bx}(m)\delta_{bx}(m)$$
(30)

$$\hat{i}_{Lx}(m) = i_{Lx}(m) - \alpha i_{Lx}(m-1)$$
(31)

$$\hat{u}_{bx}(m) = u_{bx}(m) - \alpha u_{bx}(m-1) \quad (32)$$

D. Calculation of Reference Three Phase Grid Current

Average and resultant active weights are computed as follows

$$\delta_{ava} = \frac{1}{3}\sum_{x=R,Y,B}\delta_{ax}$$
(33)

$$\delta_a = \delta_{ava} + \delta_{ca} - \delta_{pv}$$
(34)

where δ_{ava} is the average active weight, δ_a is the resultant active weight, and δ_{pv} is the feed forward term.

Similarly average and resultant reactive weights are computed as

$$\delta_{avb} = \frac{1}{3}\sum_{x=R,Y,B}\delta_{bx}$$
(35)

$$\delta_b = \delta_{cb} - \delta_{avb}$$
(36)

where x represents R, Y and B phases respectively.

The resultant active weight (δ_a) and reactive weight (δ_b) determine the active (i^*_{ax}) and reactive (i^*_{bx}) reference grid currents.

$$i^*_{ax} = \delta_a u_{ax} \quad (37)$$

$$i^*_{bx} = \delta_b u_{bx}$$
(38)

where x represents R, Y and B phases respectively.

Then the total reference grid currents are computed as

$$i^*_x = i^*_{ax} + i^*_{bx}$$
(39)

Here x represents R, Y and B phases and i^*_x represents reference grid currents of respective phases.

After generating the reference grid currents (i^*_R, i^*_Y, i^*_B) they are compared with the actual grid currents (i_R, i_Y, i_B) sensed at the point of common coupling. The error is then passed through a hysteresis band of width 0.01 for generating the gate pulses.

IV. SIMULATION RESULTS

Modelling and simulation of 50KW PV integrated system is carried out using MVSA algorithm in MATLAB/SIMULINK environment. Performance of the system is studied under various dynamic conditions. Parameters of the system under study are given in appendix.

A. Performance Analysis under Steady State

Fig.5 depicts the behaviour of the system under steady state with a nonlinear load. The responses of grid voltage (v_{RYB}), grid current (i_{RYB}), reference grid current (i^*_{RYB}), current through voltage source converter (i_{VSC}), load current (i_{LRYB}), voltage across dc link capacitor (V_{DC}), grid active (P_g) and reactive (Q_g) power, load power (P_L) and PV power (P_{PV}), current (I_{PV}) are shown. It is observed that the voltage across dc capacitor is maintained at 700V, zero grid reactive power indicates the power transfer under unity power factor condition, power transfer from source to grid is achieved after full filling the load demand.

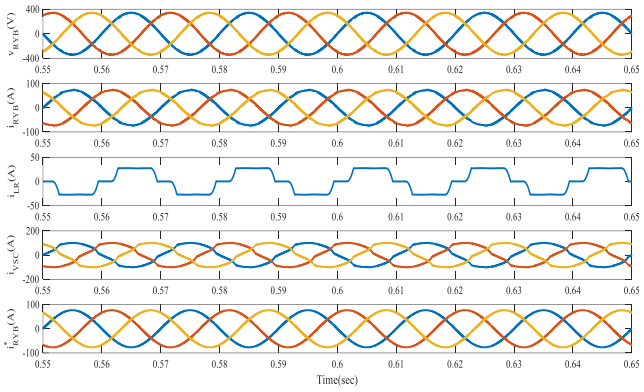

(a)

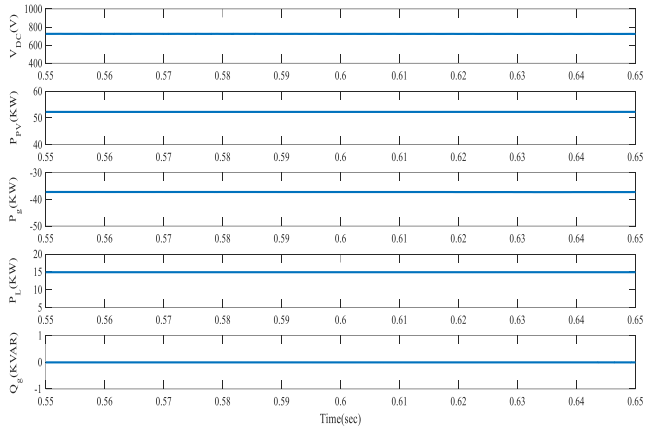

(b)

Fig.5. Simulation results under Steady State

B. Performance Analysis under Unbalanced Loading

Fig.6 depicts the behavior of the system under load unbalancing. Load unbalancing is realized during the period 0.7 to 0.9 sec. At 0.7 sec. phase R is disconnected, thus making the system unbalanced and again it is reconnected at 0.9 second. During this period R phase load current i_{LR} becomes zero. Grid voltage (v_{RYB}) and grid current (i_{RYB}) remain sinusoidal during this period. Grid current track it's reference value properly. DC link voltage (V_{DC}) maintain its value constant as defined by MPPT control.

PV power (P_{PV}) and current (I_{PV}) maintain their values constant during this period. Active power fed to the grid (P_g) increases and reactive power (Q_g) remain zero which depicts the UPF operation. The active weights $(\delta_{ava}, \delta_{ca})$ regain their values after the disturbance and the weight δ_{PV} remain constant.

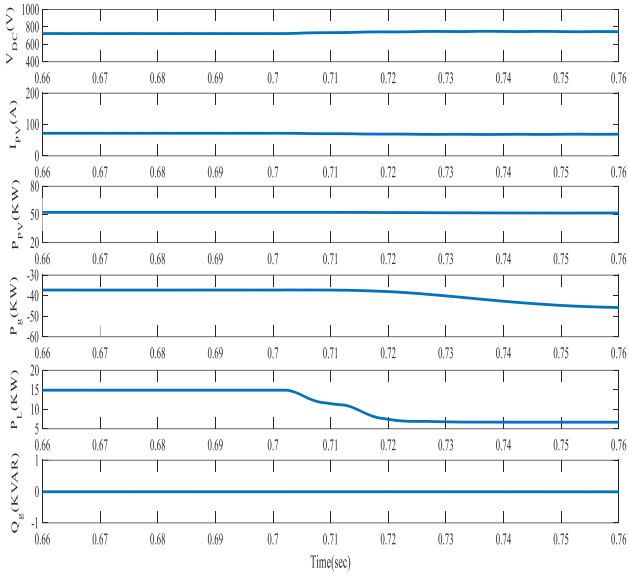

(a)

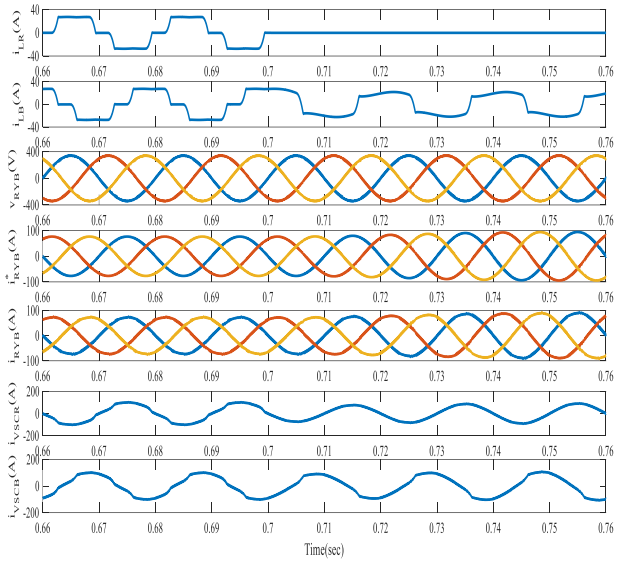

(b)

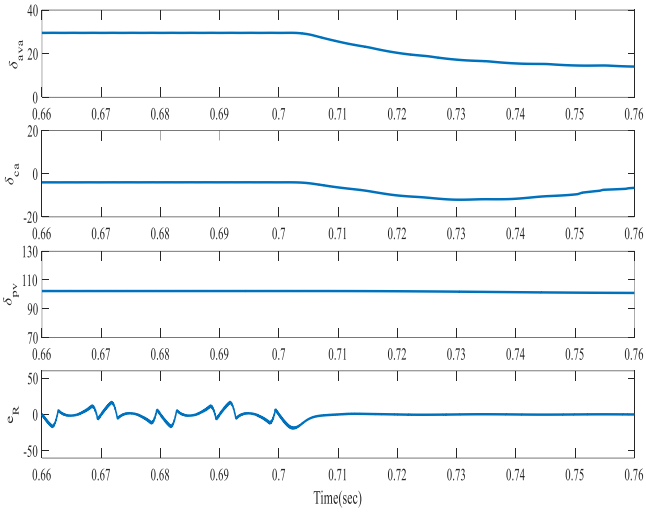

(c)

Fig.6. Simulation results under Unbalanced Loading.

C. Performance Analysis under Variable irradiation

Fig. 7 depicts the behavior of the system under variable irradiation condition. Irradiation (G) is changed from 1000W/m^2 to 500 W/m^2 at 0.4 sec. There is no variation in grid voltage (V_{RYB}) and load current (i_{LR}) is observed. With decrease in irradiation, current (I_{PV}) decreases. Hence decrease in PV power (P_{PV}) is observed during this period. As PV power is reduced due to decrease in irradiation, power supplied to the grid (P_g) is reduced but the load power (P_L) remain constant.

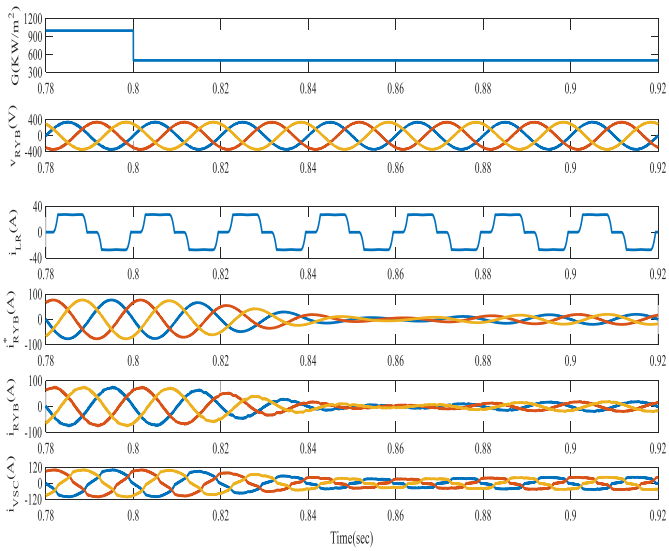

(a)

Retrieval Number: A1881109119/2019©BEIESP
DOI: 10.35940/ijeat.A1881.109119
Journal Website: www.ijeat.org

Published By:
Blue Eyes Intelligence Engineering
& Sciences Publication

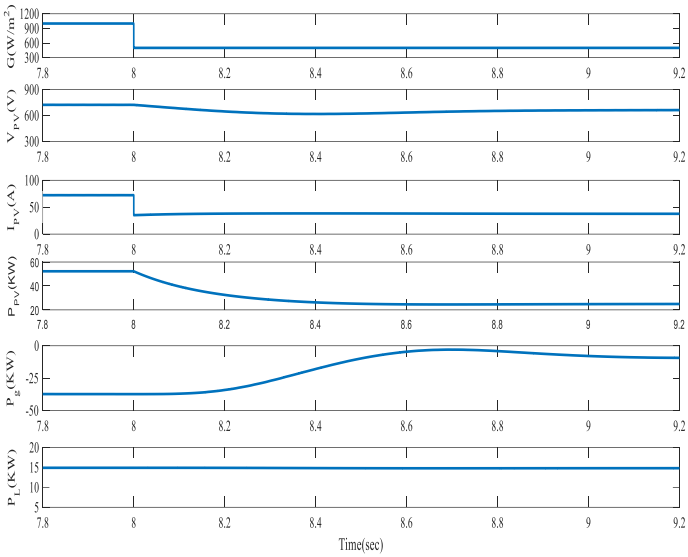

(b)

Fig.7 Simulation results under variable solar insolation

D. Comparison between MVSA and Fixed step size (FSA) algorithm

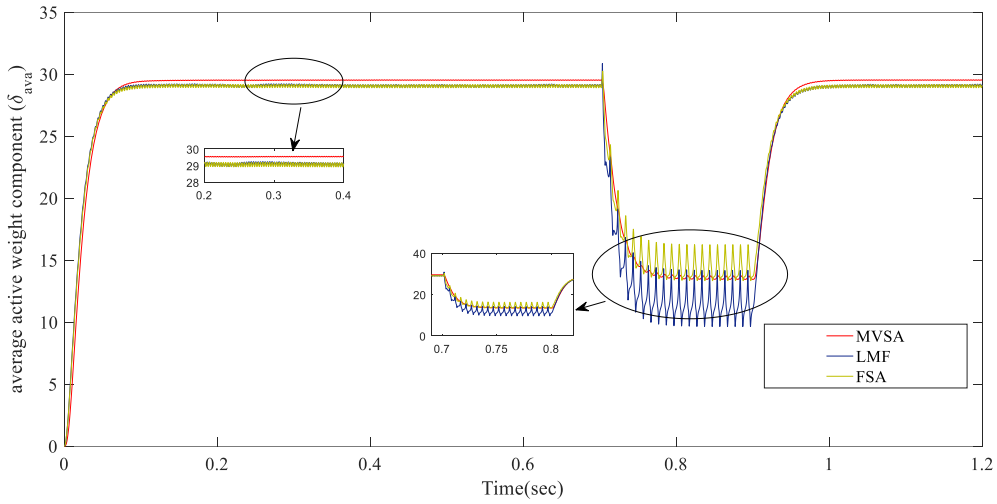

Fig. 8 shows the simulation result of MVSA, fixed step size affine (FSA) and LMF algorithm based PV integrated system.

The simulated result describes the performance of the system through the variation of Fig. 8 Response of average active weight component (δ_{ava}) of MVSA, FSA and LM the estimated average active weight (δ_{ava}) .In VSS algorithm step size is estimated at each instant, where as in FSS algorithm it is fixed. From figure.8 it is observed that the oscillation during unbalance period is almost zero in the proposed MVSA algorithm. In FSA algorithm for higher value of step size oscillation is more but for lower step size oscillation is reduced. Again the proposed algorithm shows better convergence as compared to FSA algorithm. Comparative analysis between proposed variable step size and fixed step size algorithm is given in Table 1.

Table-I Comparison of proposed MVSA, FSA and LMF

Parameters	LMF	FSA	MVSA
Step Size	Fixed	Fixed	Variable
Convergence Rate	Moderate	Moderate	Fast
Oscillations	High	Low	Almost zero

E. THD Analysis of Grid Parameters

Table 2 shows the THD data for grid voltage, grid current, load current and current through VSC as 0.79%, 2.95%, 23.73% and 7.46%.

Table-II Harmonic Analysis under UPF mode

Signal Name	Amplitude	%THD
Grid Voltage(V_{RYB})	339	0.79
Grid Current(i_{RYB})	68.26	2.95
Load Current(i_{LRYB})	29.92	23.73
VSC Current(i_{VSC})	98.14	7.46

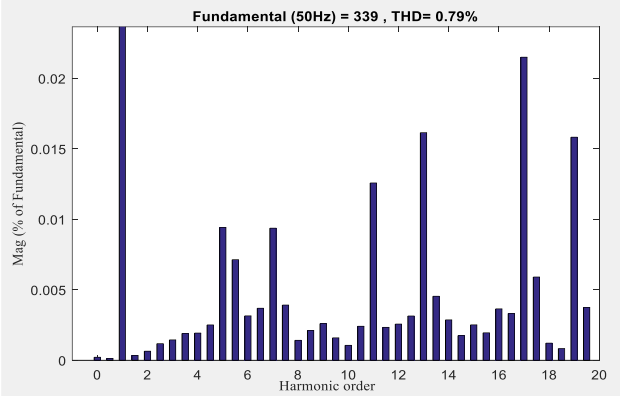

(a)

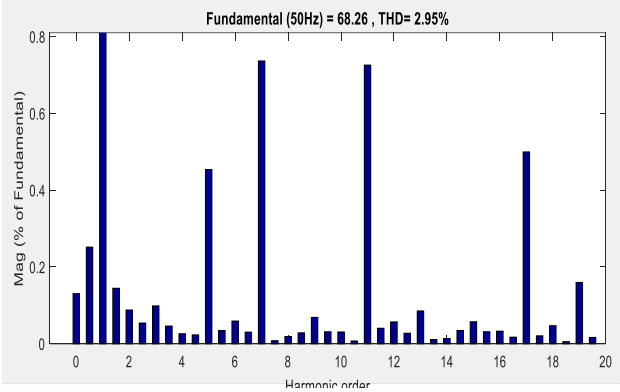

(b)

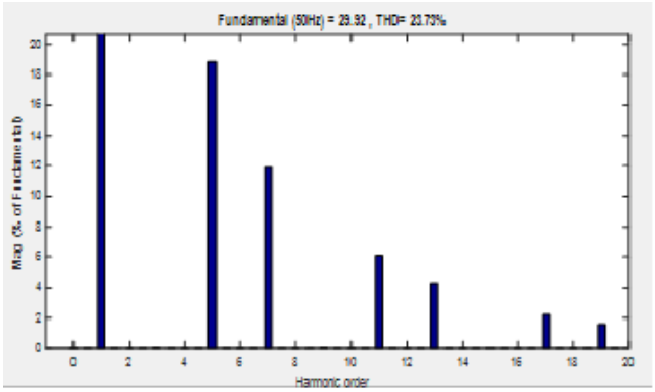

(c)

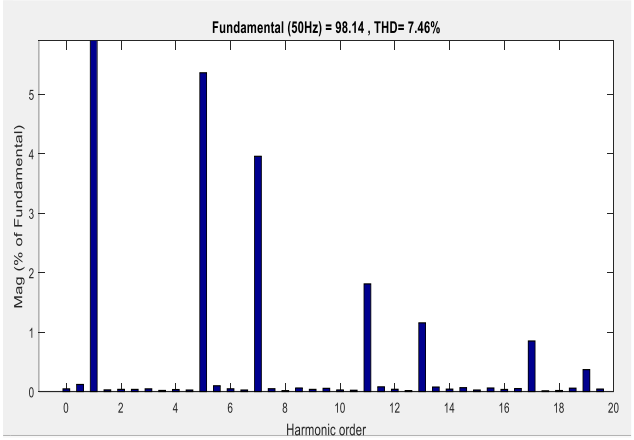

(d)

Fig.9. Harmonic analysis of grid signals (a) grid voltage (b) grid current (c) load current (d) VSC current

V. CONCLUSION

A 50KW PV-grid integrated single stage system is considered for supplying power to the non-linear load using MVSA algorithm. Dynamic stability of the system is analysed under variable irradiation and unbalanced loading condition. Performance of the proposed system is found to be better as compared to the fixed size algorithm. Oscillation of the estimated weight of the proposed system is found to be almost zero during both dynamic and steady state condition. Power transfer takes place under unity power factor irrespective of disturbances. From simulation results it is found that the THD of grid parameters are within the limit specified by IEEE-519 standard code [26].

APPENDIX

Grid integrated PV system specifications:
PV voltage (V_{PV}) = 700V, PV power = 50KW, Number of PV modules in series (N_s) = 27, Number of PV modules in parallel (N_p) = 10, DC link capacitor (C_{DC}) = 9000µF, Interfacing inductor (L)=4mH, proportional gain (k_p) = 1, Integral gain (k_i) = 0.001, scaling factor (β) = 0.9, Line voltage at grid (v_{RYB})= 415V, sampling time (T_s) = 10^{-6} seconds. Nonlinear Load: Full bridge rectifier with RL (R=20Ω, L= 100 mH) load

REFERENCES

1. IEA-ETSAP and IRENA: 'Solar Photovoltaics: Technology brief' Technical report, Energy Technology Systems Analysis Programme and international Renewable Energy Agency, Jan.2013.
2. M. G. Villalva, J. R. Gazoli and E. R. Filho, "Comprehensive Approach to Modeling and Simulation of Photovoltaic Arrays," *IEEE Transactions on Power Electronics*, vol. 24, May 2009, pp. 1198-1208.
3. D. Sera, L. Mathe, T. Kerekes, S. V. Spataru and R. Teodorescu, "On the Perturb-and-Observe and Incremental Conductance MPPT Methods for PV Systems," *IEEE Journal of Photovoltaics*, vol. 3, July 2013, pp. 1070-1078.
4. K. H. Hussein, I. Muta, T. Hoshino and M. Osakada, "Maximum photovoltaic power tracking: an algorithm for rapidly changing atmospheric conditions," *IEE Proceedings - Generation, Transmission and Distribution*, vol. 142, Jan.1995, pp. 59-64.

5. Q. Mei, M. Shan, L. Liu and J. M. Guerrero, "A Novel Improved Variable Step-Size Incremental-Resistance MPPT Method for PV Systems," *IEEE Transactions on Industrial Electronics*, vol. 58, June 2011, pp. 2427-2434.
6. K. Sundareswaran, P. Sankar, P. S. R. Nayak, S. P. Simon and S. Palani, "Enhanced Energy Output From a PV System Under Partial Shaded Conditions Through Artificial Bee Colony," *IEEE Transactions on Sustainable Energy*, vol. 6, Jan 2015, pp. 198-209.
7. C. Wei, Z. Zhang, W. Qiao and L. Qu, "Reinforcement-Learning-Based Intelligent Maximum Power Point Tracking Control for Wind Energy Conversion Systems," *IEEE Transactions on Industrial Electronics*, vol. 62, Oct 2015, pp. 6360-6370, Oct. 2015.
8. V. Baghel, "A Survey on Maximum Power Point Algorithms for PV System," *2018 Second International Conference on Electronics, Communication and Aerospace Technology (ICECA)*, Coimbatore, 2018, pp. 84-88.
9. T. L. Nguyen and K. Low, "A Global Maximum Power Point Tracking Scheme Employing DIRECT Search Algorithm for Photovoltaic Systems," *IEEE Transactions on Industrial Electronics*, vol. 57, Oct.2010, pp. 3456-3467.
10. A. K. Barnes, J. C. Balda and C. M. Stewart, "Selection of converter topologies for distributed energy resources," *2012 Twenty-Seventh Annual IEEE Applied Power Electronics Conference and Exposition (APEC)*, Orlando, FL, 2012, pp. 1418-1423.
11. J. Cioffi and T. Kailath, "Fast, recursive-least-squares transversal filters for adaptive filtering," *IEEE Transactions on Acoustics, Speech, and Signal Processing*, vol. 32, April 1984, pp. 304-337.
12. C. Lee, R. Jiang and P. Cheng, "A Grid Synchronization Method for Droop-Controlled Distributed Energy Resource Converters," *IEEE Transactions on Industry Applications*, vol. 49, March-April 2013, pp. 954-962.
13. R. K. Agarwal, I. Hussain and B. Singh, "LMF-Based Control Algorithm for Single Stage Three-Phase Grid Integrated Solar PV System," *IEEE Transactions on Sustainable Energy*, vol. 7, Oct.2016, pp. 1379-1387.
14. A. K. Pradhan, A. Routray and A. Basak, "Power system frequency estimation using least mean square technique," *IEEE Transactions on Power Delivery*, vol. 20,July 2005, pp. 1812-1816.
15. B. Subudhi, P. K. Ray and S. Ghosh, "Variable leaky least mean-square algorithm-based power system frequency estimation," *IET Science, Measurement & Technology*, vol. 6, July 2012, pp. 288-297.
16. B. Singh, C. Jain and S. Goel, "ILST Control Algorithm of Single-Stage Dual Purpose Grid Connected Solar PV System," in *IEEE Transactions on Power Electronics*, vol. 29, Oct. 2014, pp. 5347-5357.
17. K Ozeki, T Umeda.'An adaptive filtering algorithm using an orthogonal projection to an affine subspace and its properties', *Electron. Commun. Jpn.*, 1984, 67-A, (5), pp. 19-27.
18. M Abadi, A Gholipour, V Mehrdad.' A family of variable step-size affine projection adaptive filtering algorithms with selective regressors', *International Journal of signal and Image Processing*, 2010, 6, (1), pp.108-120.
19. A Mader, H Puder, G U Schmidt.: ' Step-size control for acoustic echo cancellation filters-an overview, *signal Processing*. 2000, 80, pp.1697-1719.
20. Hyun-Chool Shin, A. H. Sayed and Woo-Jin Song, "Variable step-size NLMS and affine projection algorithms," *IEEE Signal Processing Letters*, vol. 11, Feb. 2004, pp. 132-135.
21. H. Rey, L. R. Vega, S. Tressens and J. Benesty, "Variable Explicit Regularization in Affine Projection Algorithm: Robustness Issues and Optimal Choice," *IEEE Transactions on Signal Processing*, vol. 55,May 2007, pp. 2096-2109.
22. Mohan N, Undeland TM, Robbins WP.: *'Power Electronics: converters Applications and Design*', 2003,New York, NY, USA: wiley.
23. H Akagi, EH Watanabe, M Aredes. *Instantaneous Power Theory and applications to power Conditioning*, 2007,New York, NY, USA; Wiley.
24. B Singh, A Chandra, K Al-Haddad. *'Power quality: problems and mitigation techniques*' 2015,John Wiley & Sons.
25. J. Hwang and Y. Li, "Variable Step-Size LMS Algorithm With a Gradient-Based Weighted Average," in *IEEE Signal Processing Letters*, vol. 16, Dec.2009, pp. 1043-1046.
26. IEEE recommended practice and requirements for harmonic control in electrical power system, IEEE std. 519, 1992.